JOURNAL OF THERMOPHYSICS AND HEAT TRANSFER
Vol. 20, No. 4, October–December 2006

Technical Notes

TECHNICAL NOTES are short manuscripts describing new developments or important results of a preliminary nature. These Notes should not exceed 2500 words (where a figure or table counts as 200 words). Following informal review by the Editors, they may be published within a few months of the date of receipt. Style requirements are the same as for regular contributions (see inside back cover).

Effects of Joule Heating on Electrohydrodynamics-Enhanced Natural Convection in an Enclosure

M. Huang* and F. C. Lai†
University of Oklahoma, Norman, Oklahoma 73019

DOI: 10.2514/1.17848

Nomenclature

b = ion mobility of air, $b = 1.43 \times 10^{-4}$ m^2/V · s for positive ions in air
c_p = heat capacity, J/kg · K
$\boldsymbol{D}$ = electric flux vector, C/m^2
$\boldsymbol{E}$ = electric field vector, V/m
E_x = x-component of electric field, V/m
g = gravitational acceleration, m/s^2
H = height of the enclosure, m
I_{cal} = corona current on the grounded wall as calculated from numerical simulation, A
$\boldsymbol{J}$ = current density vector, A/m^2
L = width of the enclosure, m
L_w = length of the wire electrode, m
N_{EHD} = electrohydrodynamics number, Eq. (22)
Nu = average Nusselt number in the presence of an electric field, Eq. (19)
Nu_x = local Nusselt number, Eq. (18)
Nu_0 = average Nusselt number in the absence of an electric field
$\overline{Nu}$ = time-averaged Nusselt number, Eqs. (20) and (21)
Pe_{EHD} = electric Peclet number, $u_e L/\alpha$
Pr = Prandtl number
p = pressure, Pa
Ra = Rayleigh number, $g\beta(T_h - T_c)L^3/\alpha\nu$
Re_{EHD} = electric Reynolds number, $u_e L/\nu$
T = temperature, K
t = time, s
u = x component of velocity, m/s
u_c = characteristic velocity of thermal buoyancy, $g\beta(T_h - T_c)L^2/\nu$, m/s
u_e = characteristic velocity of ionic wind, $\sqrt{\rho_{c0}V_0/\rho}$, m/s
V = electric potential, V
$\bar{V}$ = dimensionless electric potential, V/V_0
V_0 = electric potential at the wire, V
v = y component of velocity, m/s
X, Y = dimensionless Cartesian coordinates
x, y = Cartesian coordinates, m
α = thermal diffusivity, m^2/s
β = coefficient of thermal expansion, 1/K
ε_0 = permittivity of free space, $\varepsilon_0 = 8.854 \times 10^{-12}$ F/m
θ = dimensionless temperature, $(T - T_c)/(T_h - T_c)$
ν = kinematic viscosity, m^2/s
ρ = density, kg/m^3
ρ_c = charge density, C/m^3
ρ_{c0} = charge density at the wire, C/m^3
$\overline{\rho_c}$ = dimensionless charge density, ρ_c/ρ_{c0}
τ = dimensionless time, $u_e t/L$
τ_P = dimensionless period of an oscillatory flow
τ_1 = characteristic time in the calculation of a time-averaged Nusselt number
Ψ = dimensionless stream function
Ω = dimensionless vorticity

Subscripts

c = cold wall
h = hot wall

Introduction

HEAT transfer enhancement in natural convection by electrohydrodynamics (EHD) was first investigated as early as 1962 [1]. All subsequent studies have confirmed the effectiveness of heat transfer enhancement using an electric field (e.g., Marco and Velkoff [2], Franke [3], Yabe et al. [4], as well as Franke and Huston [5]). Because of the complexities involved, previous studies on EHD-enhanced heat transfer were mostly conducted by experiment. Although some success has been recently reported in the numerical solution of such problems [6–8], these attempts have generally neglected the effects of Joule heating. For forced convection, Joule heating may be small enough to justify its negligence, but its effects on natural convection have never been properly quantified and documented. Thus, it is the objective of this study to evaluate the effects of Joule heating on the heat transfer enhancement in natural convection using an electric field. In addition, their effects over the stability of flow and temperature fields are also investigated.

Formulation and Numerical Method

The geometry considered is a two-dimensional enclosure with a height of 0.508 m (20 in.) and a width of 0.102 m (4 in.), which is exactly the same as that used in the study by Tan and Lai [9]. The enclosure is filled with air. Whereas the top and bottom walls are electrically and thermally insulated, the two vertical walls are electrically grounded and maintained at constant temperatures, T_h and T_c ($T_h > T_c$), respectively. A copper wire of 0.5-mm diameter charged with a positive direct current at a high voltage is placed inside the enclosure at three different locations (Fig. 1). Although Tan and Lai [9] have shown that an electrode should be placed as close to the wall as possible to achieve the best result in heat transfer enhancement using an electric field, the present wire location is selected for ease in quantifying the effect of Joule heating. Three positive potentials (relative to the grounded surface) at 12, 15, and 18 kV are applied to the wire to create the electric field.

The governing equations for the electric field are [10]

Received 24 May 2005; revision received 15 February 2006; accepted for publication 24 February 2006.

*Graduate Research Assistant, School of Aerospace and Mechanical Engineering.
†Associate Professor, School of Aerospace and Mechanical Engineering; flai@ou.edu. Associate Fellow AIAA.

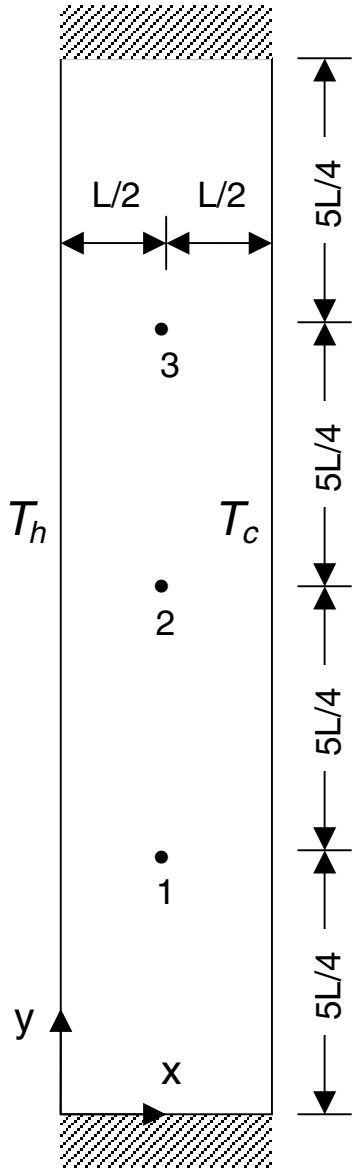

Fig. 1 A two-dimensional enclosure with a wire electrode placed at three different positions.

the Maxwell equation

$$\nabla \cdot \boldsymbol{D} = \rho_c \tag{1}$$

the current continuity equation

$$\nabla \cdot \boldsymbol{J} = 0 \tag{2}$$

and Ohm's law

$$\boldsymbol{J} = \rho_c b \boldsymbol{E} \tag{3}$$

In the formulation of Ohm's law, the contribution to current density by convective transport of charge is assumed negligible, which is justifiable because the ion drift velocity is usually much greater than the bulk fluid velocity induced by thermal buoyancy. This assumption leads to the so-called one-way coupling between the electric and flowfields (that is, the electric field has influences over the flowfield, but not vice versa). As a result, the governing equations for the electric field can be solved independently of the flow and temperature fields. For a positive corona, the electric discharge is uniformly distributed along the wire and is inherently stable so that it can be assumed two-dimensional.

With the definitions $\boldsymbol{D} = \varepsilon_0 \boldsymbol{E}$ and $\boldsymbol{E} = -\nabla V$, Eq. (1) can be rearranged to give

$$\frac{\partial^2 V}{\partial x^2} + \frac{\partial^2 V}{\partial y^2} = -\frac{\rho_c}{\varepsilon_0} \tag{4}$$

Combining Eqs. (3) and (4), one can rewrite the current continuity equation in the following form:

$$\left(\frac{\partial \rho_c}{\partial x}\frac{\partial V}{\partial y} + \frac{\partial \rho_c}{\partial y}\frac{\partial V}{\partial x}\right) = \frac{\rho_c^2}{\varepsilon_0} \tag{5}$$

To determine the electric field, the reduced Maxwell Eq. (4) and the current continuity Eq. (5) must be solved simultaneously, subject to the following boundary conditions:

at the wire

$$V = V_o \tag{6}$$

along the grounded walls

$$V = 0 \tag{7}$$

along the insulated walls

$$\frac{\partial V}{\partial y} = 0 \tag{8}$$

For flow and temperature fields, the governing equations are given by

$$\frac{\partial u}{\partial x} + \frac{\partial v}{\partial y} = 0 \tag{9}$$

$$\frac{\partial u}{\partial t} + u\frac{\partial u}{\partial x} + v\frac{\partial u}{\partial y} = -\frac{1}{\rho}\frac{\partial p}{\partial x} + \nu\left(\frac{\partial^2 u}{\partial x^2} + \frac{\partial^2 u}{\partial y^2}\right) - \frac{\rho_c}{\rho}\frac{\partial V}{\partial x} \tag{10}$$

$$\frac{\partial v}{\partial t} + u\frac{\partial v}{\partial x} + v\frac{\partial v}{\partial y} = -\frac{1}{\rho}\frac{\partial p}{\partial y} + \nu\left(\frac{\partial^2 v}{\partial x^2} + \frac{\partial^2 v}{\partial y^2}\right) + g\beta(T - T_c) - \frac{\rho_c}{\rho}\frac{\partial V}{\partial y} \tag{11}$$

$$\frac{\partial T}{\partial t} + u\frac{\partial T}{\partial x} + v\frac{\partial T}{\partial y} = \alpha\left(\frac{\partial^2 T}{\partial x^2} + \frac{\partial^2 T}{\partial y^2}\right) + \frac{b\rho_c}{\rho c_p}\left[\left(\frac{\partial V}{\partial x}\right)^2 + \left(\frac{\partial V}{\partial y}\right)^2\right] \tag{12}$$

Whereas the last term in Eqs. (10) and (11) represents the electric body force, the third term on the right hand side of Eq. (11) is thermal buoyancy. The last term in the energy equation Eq. (12) accounts for the Joule heating [10].

The preceding governing equations can be cast into the dimensionless form in terms of stream function and vorticity and they are given by [11]

$$\frac{\partial^2 \Psi}{\partial X^2} + \frac{\partial^2 \Psi}{\partial Y^2} = -\Omega \tag{13}$$

$$\frac{\partial \Omega}{\partial \tau} + \frac{\partial \Psi}{\partial Y}\frac{\partial \Omega}{\partial X} - \frac{\partial \Psi}{\partial X}\frac{\partial \Omega}{\partial Y} = \frac{1}{Re_{\mathrm{EHD}}}\left(\frac{\partial^2 \Omega}{\partial X^2} + \frac{\partial^2 \Omega}{\partial Y^2}\right) + \frac{RaPr}{Pe_{\mathrm{EHD}}^2}\frac{\partial \theta}{\partial X} + \left(\frac{\partial \bar{V}}{\partial Y}\frac{\partial \overline{\rho_c}}{\partial X} - \frac{\partial \bar{V}}{\partial X}\frac{\partial \overline{\rho_c}}{\partial Y}\right) \tag{14}$$

$$\frac{\partial \theta}{\partial \tau} + \frac{\partial \Psi}{\partial Y}\frac{\partial \theta}{\partial X} - \frac{\partial \Psi}{\partial X}\frac{\partial \theta}{\partial Y} = \frac{1}{Pe_{\mathrm{EHD}}}\left(\frac{\partial^2 \theta}{\partial X^2} + \frac{\partial^2 \theta}{\partial Y^2}\right) + \frac{b\rho_c V_0^2}{\rho c_p u_e L(T_h - T_c)}\left[\left(\frac{\partial \bar{V}}{\partial X}\right)^2 + \left(\frac{\partial \bar{V}}{\partial Y}\right)^2\right] \tag{15}$$

The coefficient of the last term in the energy equation, Eq. (15),

represents the ratio of Joule heating to the thermal energy convected by the corona wind. Apparently, if this value is small, then the effects of Joule heating are negligible.

The corresponding boundary conditions for the flow and temperature fields are

$$X = 0, \qquad \Omega = \frac{\partial^2 \Psi}{\partial X^2}, \qquad \Psi = 0, \qquad \theta = 1 \tag{16a}$$

$$X = 1, \qquad \Omega = \frac{\partial^2 \Psi}{\partial X^2}, \qquad \Psi = 0, \qquad \theta = 0 \tag{16b}$$

$$Y = 0, \qquad \Omega = \frac{\partial^2 \Psi}{\partial Y^2}, \qquad \Psi = 0, \qquad \frac{\partial \theta}{\partial Y} = 0 \tag{16c}$$

$$Y = 5, \qquad \Omega = \frac{\partial^2 \Psi}{\partial Y^2}, \qquad \Psi = 0, \qquad \frac{\partial \theta}{\partial Y} = 0 \tag{16d}$$

The numerical solutions begin with the calculation of the electric field, followed by solving the flow and temperature fields simultaneously. The numerical scheme used to calculate the electric field is the same as that proposed by Yamamoto and Velkoff [12]. With this scheme, the total current on the grounded wall is required (which is used as the convergence criterion for numerical calculations as will be explained in the following discussion) and must be obtained from experiment. To begin, the potential distribution is first calculated using Eq. (4) with the assumption that no charge is present initially. Once the potentials become available, the charge density distribution over the entire enclosure can be calculated using Eq. (5) with an initial guess of the charge density at the wire. Subsequently, the potential distribution is recalculated using Eq. (4) and the value of the charge density just obtained. The total current on the grounded wall is then calculated from the following equation, and compared with the total current determined from experiment.

$$I_{\text{cal}} = \int_0^H \rho_c E_x b L_w \, \mathrm{d}y \tag{17}$$

If they are different, a new charge density at the wire is assumed and the process is repeated until the calculated total current is converged to that experimentally measured.

Because the present geometry is exactly the same as that used by Tan and Lai [9], the electric field data from their experiment are used in the present numerical solution of an electric field. It should be mentioned that there are other numerical schemes available in the literature for the calculation of an electric field with corona discharge (for example, McDonald et al. [13]). Although these schemes may not require experimental corona current data in the numerical solutions, they usually involve empirical constants that have to be determined by experiments or simply based on the judgment of the user. Because these empirical constants are not rigorously defined, the approach proposed by Yamamoto and Velkoff [12] is preferred in the present study. As reported by Tan and Lai [9], the agreement between the numerical prediction and experimental measurement of the electric field is excellent.

The solutions for the flow and temperature fields are obtained using the standard vorticity-stream function method. A grid refinement test was conducted before the production run. It was concluded that a uniform grid of 101×501 with a dimensionless time step of 5×10^{-4} is best for the present study in terms of accuracy and computational cost [11]. The code for the solutions of flow and temperature fields was validated against those reported by Schinkel et al. [14] for pure natural convection in a rectangular enclosure. In addition, the heat transfer results in terms of the average Nusselt number were compared with the correlation proposed by Berkovsky and Polevikov [15]. It was found that the agreement was very good with a discrepancy of only 1.6% at $Ra = 10^6$. To verify that the observed oscillations are not due to numerical instability, some calculations are repeated and verified with a reduced time step $\Delta\tau = 1 \times 10^{-4}$ and a finer mesh of 161×801.

To evaluate the heat transfer rate, the local heat transfer coefficient is expressed in terms of the local Nusselt number:

$$Nu = -\left(\frac{\partial \theta}{\partial X}\right)_{X=0,1} \tag{18}$$

The spatially averaged Nusselt number is then determined from the local heat flux by

$$Nu = \frac{1}{5}\int_0^5 Nu_x \, \mathrm{d}Y \tag{19}$$

Because the flow and temperature fields under the influence of electric field may become oscillatory, the Nusselt number needs to be defined differently for these special cases. For periodic flows, the time-averaged Nusselt number is calculated by averaging the Nusselt number over the period of oscillation and is given by

$$\overline{Nu} = \frac{1}{\tau_P}\int_\tau^{\tau+\tau_P} Nu \, \mathrm{d}\tau \tag{20}$$

where the Nusselt number is defined in Eq. (19). For nonperiodic flows, the time-averaged Nusselt number is calculated by averaging the Nusselt number over a time span τ_1 as shown next:

$$\overline{Nu} = \frac{1}{\tau_1}\int_\tau^{\tau+\tau_1} Nu \, \mathrm{d}\tau \tag{21}$$

The preceding time averaging is performed after the initial transient settles out, which usually takes more than 200 dimensionless time units (i.e., $\tau \geq 200$), depending on the electric field strength and Rayleigh number. It has been found that the average Nusselt number for nonperiodic flows approaches an asymptotic value if it is averaged over a sufficiently long time.

Results and Discussion

For an electric field, the distributions of electric potential and charge density are shown in Fig. 2 for three wire locations. It is evident that electric potential and charge density are maximal at the wire for all positions considered. They dissipate outward and have minimal values on the vertical walls (i.e., the grounded surfaces). Charge density has a significant influence on the distribution of electric potential. If the charge were absent, the electric potential would distribute more symmetrically around the wire. With the presence of charge, the potential distribution is greatly distorted and stretched vertically.

For heat transfer, the results obtained with the effects of Joule heating generally show the same trend as those without. That is, the heat transfer enhancement by an electric field increases with increased applied voltage, but decreases with increased Rayleigh number. However, the two results differ quite significantly, particularly at low Rayleigh numbers. An earlier study [9] showed that the flow and temperature fields may develop into periodic oscillatory modes at low Rayleigh numbers ($Ra \leq 10^4$) when Joule heating is neglected. From the present study, it is shown that, with the inclusion of Joule heating, the flow and temperature fields in many of these cases have further evolved to nonperiodic oscillation. In some cases, even though the flow and temperature fields may have periodic oscillatory modes, their profiles are very different from those without Joule heating. For example, this can be observed from the flow and temperature fields shown in Figs. 3–6. The cases shown are for the flow and temperature fields going through one cycle (period) of oscillation. From the streamline contours (Figs. 3 and 4), one can clearly observe the formation and breaking up of secondary cells that lead to the oscillatory mode. Despite some similarities between the two cases, the oscillation of these two flowfields is clearly out of phase and has a slightly different period. More differences can be observed in the temperature fields from these two cases. When Joule heating is neglected, the temperature field is only perturbed by the

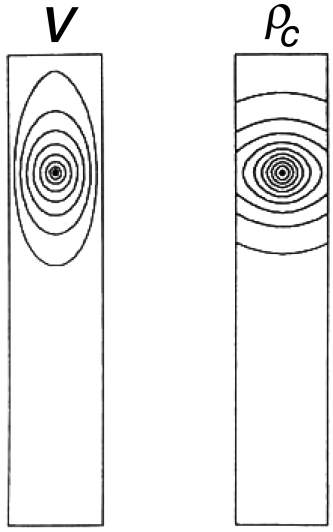

a) Wire position 3 (ρ_{c0} = 6.36 x 10^{-5} C/m^3)

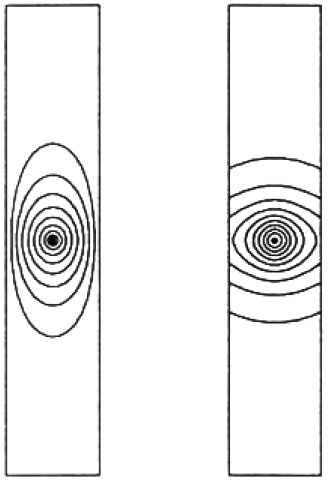

b) Wire position 2 (ρ_{c0} = 6.03 x 10^{-5} C/m^3)

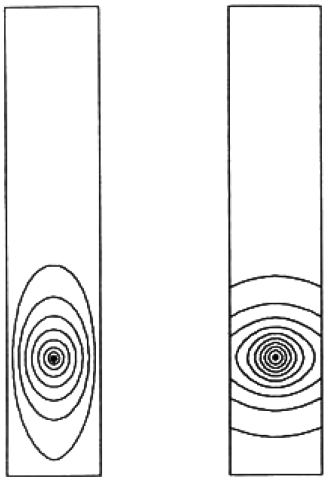

c) Wire position 1 (ρ_{c0} = 6.36 x 10^{-5} C/m^3)

Fig. 2 Distribution of electric potential and charge density at V_0 = 15 kV (ΔV = 2 kV and $\Delta \rho_c = 6 \times 10^{-6}$ C/m^3).

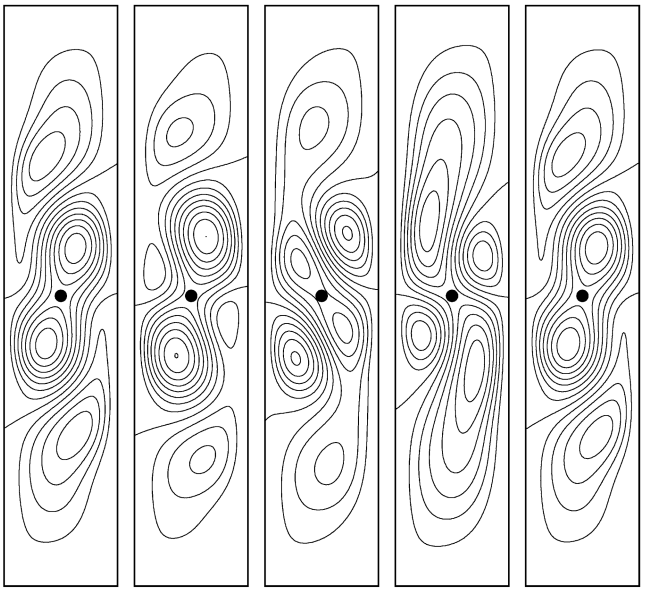

a) $\tau = 656.1$ b) $\tau = 668.6$ c) $\tau = 681.1$ d) $\tau = 693.6$ e) $\tau = 705.8$

Fig. 3 Flowfield at wire position 2 (V_0 = 12 kV, $Ra = 10^4$, without Joule heating, $\Delta\Psi = 0.005$).

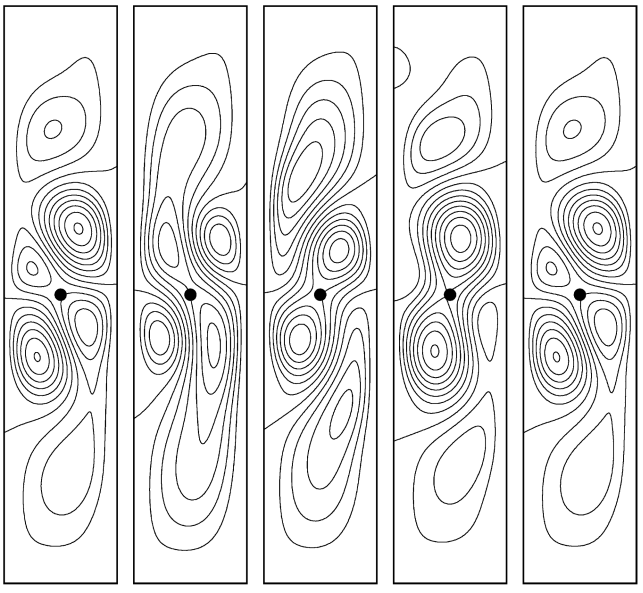

a) $\tau = 611.9$ b) $\tau = 623.9$ c) $\tau = 635.9$ d) $\tau = 647.9$ e) $\tau = 660.9$

Fig. 4 Flowfield at wire position 2 (V_0 = 12 kV, $Ra = 10^4$, with Joule heating, $\Delta\Psi = 0.005$).

electric field near the wire location (Fig. 5). The development of the thermal boundary layer is disrupted by the corona wind issued from the wire. When Joule heating is included (Fig. 6), the temperature field is not only affected by the corona wind, but also by the thermal buoyancy produced from Joule heating. Although the added thermal energy from Joule heating is normally small, it is relatively large in comparison to the heat transferred between the vertical walls when the Rayleigh number is small. As such, it produces additional thermal buoyancy from the wire. Because the distribution of charge density is most concentrated near the wire, the effect of Joule heating is also most prominent at the wire (Fig. 6). The combined effect of corona wind and thermal buoyancy resulting from Joule heating produces a very large temperature gradient at the cold wall directly opposite to the wire. From the preceding observation, one is certain that Joule heating can easily destabilize the flow and temperature fields at low Rayleigh numbers and leads to nonperiodic oscillation. In contrast, the effect of Joule heating is not as significant when the Rayleigh number is large. The inclusion of Joule heating in these cases only produces a slight change in the period of oscillation as is evident from the figures shown previously.

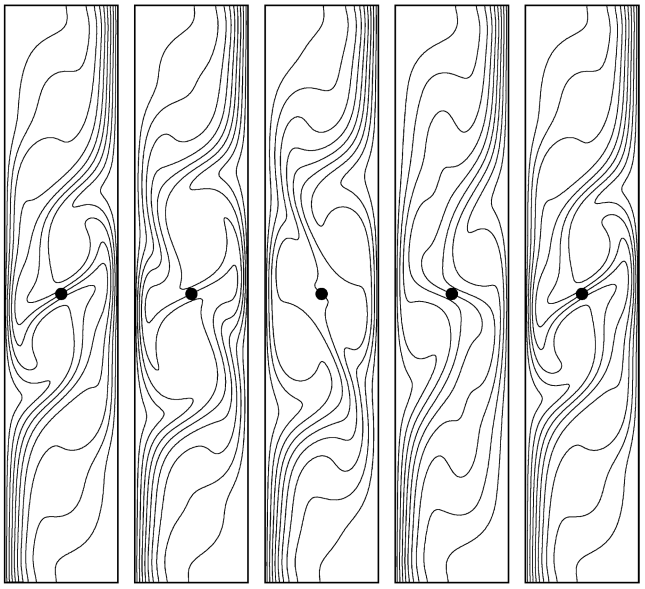

a) $\tau = 656.1$ b) $\tau = 668.6$ c) $\tau = 681.1$ d) $\tau = 693.6$ e) $\tau = 705.8$

Fig. 5 Temperature field at wire position 2 ($V_0 = 12$ kV, $Ra = 10^4$, without Joule heating, $\Delta\theta = 0.2$).

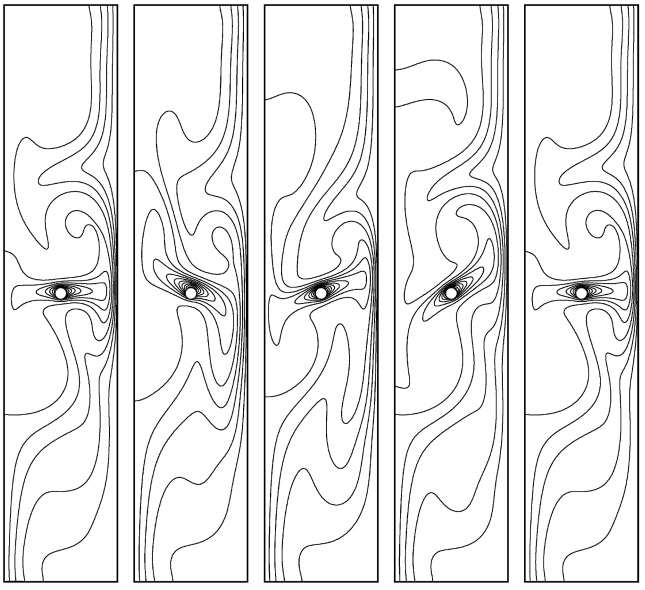

a) $\tau = 611.9$ b) $\tau = 623.9$ c) $\tau = 635.9$ d) $\tau = 647.9$ e) $\tau = 660.9$

Fig. 6 Temperature field at wire position 2 ($V_0 = 12$ kV, Ra $= 10^4$, with Joule heating, $\Delta\theta = 0.1$).

The differences in the flow and temperature fields obtained from two approaches (with and without Joule heating) diminish when the Rayleigh number increases. These can be observed from Figs. 7 and 8 when both flow and temperature fields become steady. The streamline contours show that the flowfields obtained from the two approaches are almost identical, except for the slight difference in the flow strength (Fig. 7). For temperature fields, the major difference only appears near the wire at $Ra = 10^5$ (Fig. 8). This indicates that the thermal buoyancy produced by Joule heating becomes negligible when the Rayleigh number increases. The added thermal energy from Joule heating becomes only a very small fraction of the energy transported from the differentially heated walls when the Rayleigh number is greater than 10^5.

For the present study, heat transfer enhancement by an electric field is evaluated by the ratio between the Nusselt numbers thus obtained and those of pure natural convection. The results are shown

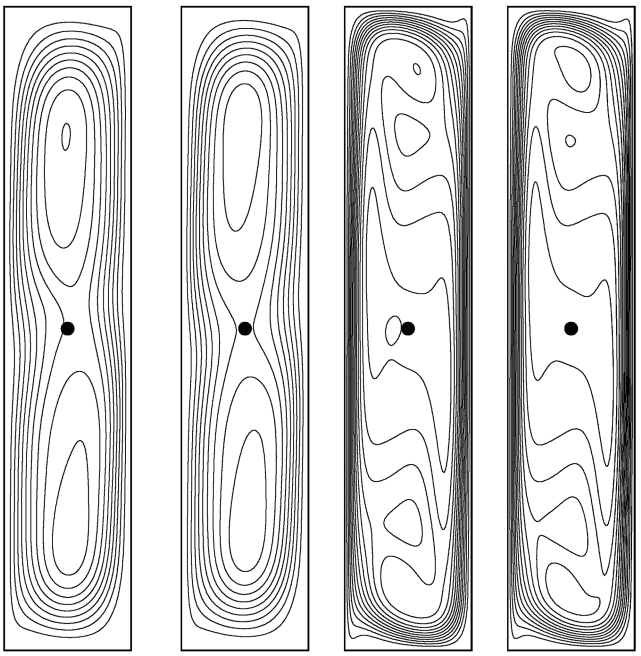

a) $Ra = 10^5$ (with Joule heating) b) $Ra = 10^5$ (without Joule heating) c) $Ra = 10^6$ (with Joule heating) d) $Ra = 10^6$ (without Joule heating)

Fig. 7 Steady flowfield at wire position 2 ($V_0 = 12$ kV, $\Delta\Psi = 0.005$).

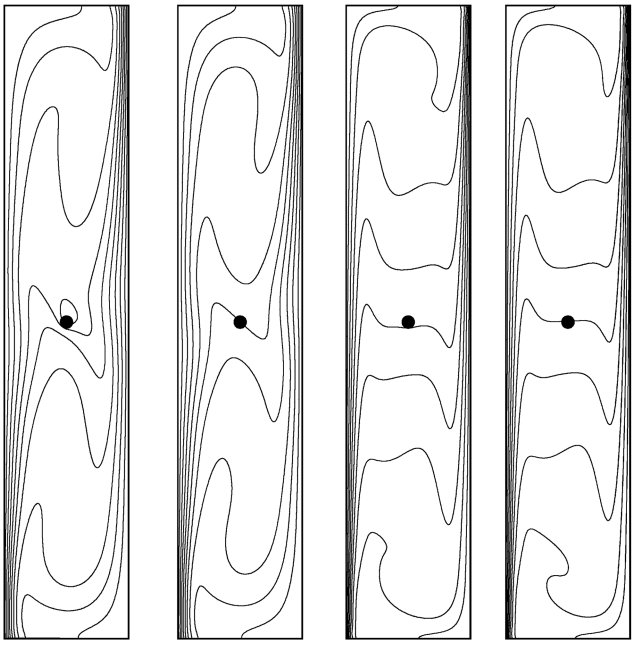

a) $Ra = 10^5$ (with Joule heating) b) $Ra = 10^5$ (without Joule heating) c) $Ra = 10^6$ (with Joule heating) d) $Ra = 10^6$ (without Joule heating)

Fig. 8 Steady temperature field at wire position 2 ($V_0 = 12$ kV, $\Delta\theta = 0.1$).

in Figs. 9 and 10, respectively, without and with Joule heating. For oscillatory cases, the maximum and minimum Nusselt numbers are shown as error bars. To evaluate the effects of electric field on natural convection, a dimensionless parameter, the EHD number N_{EHD} defined next is employed.

$$N_{\mathrm{EHD}} = \frac{Pe_{\mathrm{EHD}}}{Ra} = \frac{u_e}{u_c} \tag{22}$$

where $u_c (= g\beta(T_h - T_c)L^2/\nu)$ is the characteristic velocity of

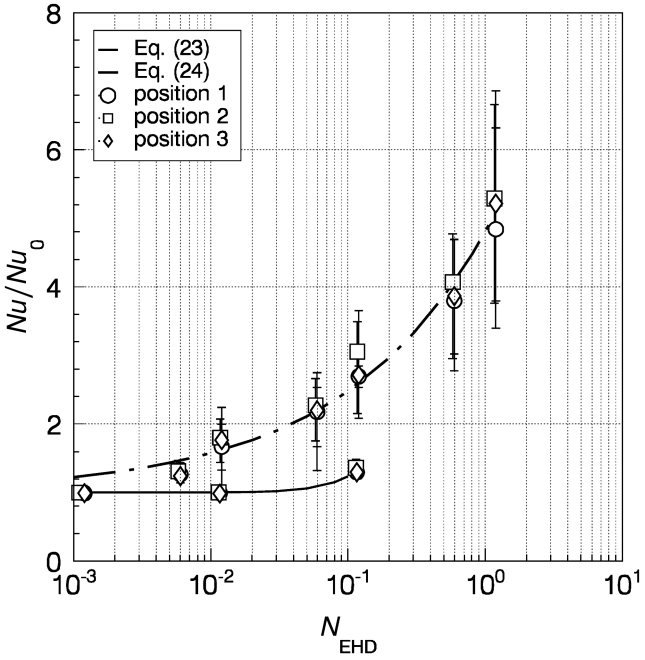

Fig. 9 Heat transfer enhancement without Joule heating.

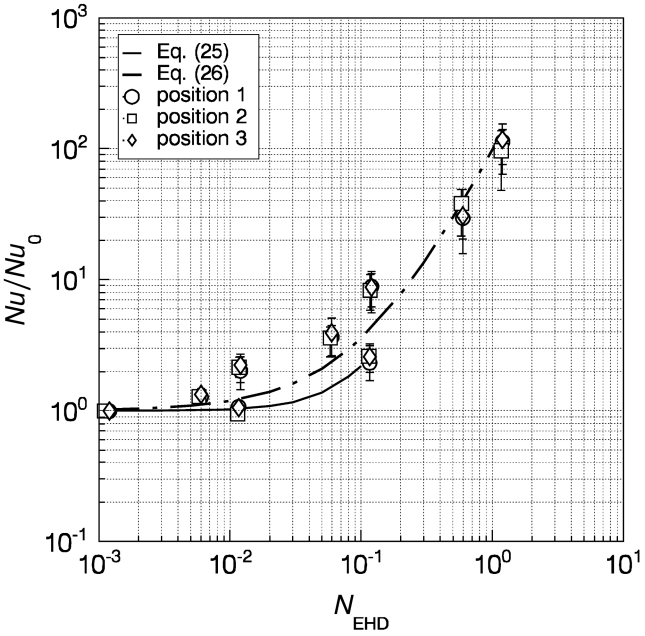

Fig. 10 Heat transfer enhancement with Joule heating.

thermal buoyancy. The EHD number thus defined is the ratio of electrical body force to thermal buoyancy. A smaller Rayleigh number or a higher applied voltage will lead to a larger EHD number.

It is clearly shown from the figures that heat transfer enhancement by an electric field can be correlated in two different forms, depending on the corona current involved. Without the effect of Joule heating, the correlations of heat transfer enhancement are given by

$$\frac{Nu}{Nu_0} = 1 + 23.660N_{\mathrm{EHD}}^2 \quad \text{for } I_{\mathrm{cal}} \le 0.73\ \mu\mathrm{A} \tag{23}$$

$$\frac{Nu}{Nu_0} = 1 + 3.806N_{\mathrm{EHD}}^{0.411} \quad \text{for } 13.72 \le I_{\mathrm{cal}} \le 38.5\ \mu\mathrm{A} \tag{24}$$

When the effect of Joule heating is included, the correlations of heat transfer enhancement are given by

$$\frac{Nu}{Nu_0} = 1 + 53.659N_{\mathrm{EHD}}^{1.655} \quad \text{for } I_{\mathrm{cal}} \le 0.73\ \mu\mathrm{A} \tag{25}$$

$$\frac{Nu}{Nu_0} = (1 + 8.914N_{\mathrm{EHD}})^2 \quad \text{for } 13.72 \le I_{\mathrm{cal}} \le 38.5\ \mu\mathrm{A} \tag{26}$$

It should be noted that the value of heat transfer enhancement reduces to unity (i.e., pure natural convection) when there is no electric field applied (i.e., $N_{\mathrm{EHD}} = 0$). Although the heat transfer results from both cases (with and without the effect of Joule heating) show the same general trend that they increase with the EHD number, there is a large discrepancy in their values, particularly at a large EHD number. As discussed earlier, this is mainly due to the additional energy provided by the electric field through Joule heating. At a small Rayleigh number (e.g., $Ra = 10^4$), the heat transfer enhancement cannot be totally accredited to corona wind. The additional thermal buoyancy produced by Joule heating is mainly responsible for this dramatic increase in the heat transfer enhancement.

Conclusion

The present study has once again confirmed that an electric field can significantly enhance heat transfer. For natural convection, the heat transfer enhancement is most notable at a low Rayleigh number. Although the heat transfer enhancement may be quite impressive at low Rayleigh numbers ($Ra \le 10^4$), one should be cautious because the added energy from an electric field (i.e., Joule heating) has contributed greatly to this heat transfer enhancement. Therefore, it is important to distinguish between the various components that have contributed to the heat transfer enhancement at low Rayleigh numbers. On the other hand, the effects of Joule heating are negligible when the Rayleigh number is large ($Ra \ge 10^5$). This is because the added electric energy is small compared with the thermal energy provided by differentially heating from vertical walls. The present study has an important implication for the experimental study of EHD-enhanced natural convection. When evaluating the heat transfer enhancement at low Rayleigh numbers, one needs to carefully identify various components to assess whether or not they actually contribute to the heat transfer enhancement. Claims of unrealistic heat transfer enhancement may result if care is not taken.

References

[1] Lykoudis, P. S., and Yu, C. P., "The Influence of Electrostrictive Forces in Natural Thermal Convection," *International Journal of Heat and Mass Transfer*, Vol. 6, No. 9, 1963, pp. 853–862.

[2] Marco, S. M., and Velkoff, H. R., "Effect of Electrostatic Fields on Free Convection Heat Transfer from Flat Plates," American Society of Mechanical Engineers Paper 63-HT-9, 1963.

[3] Franke, M. E., "Effect of Vortices Induced by Corona Discharge on Free Convection Heat Transfer from a Vertical Plate," *Journal of Heat Transfer*, Vol. 91, No. 3, 1969, pp. 427–433.

[4] Yabe, A., Mori, Y., and Hijitata, K., "EHD Study of the Corona Wind Between Wire and Plate Electrodes," *AIAA Journal*, Vol. 16, No. 4, 1978, pp. 340–345.

[5] Franke, M. E., and Huston, K. E., "Effect of Corona Discharge on the Free Convection Heat Transfer Inside a Vertical Hollow Cylinder," American Society of Mechanical Engineers Paper 82 WA/HT-20, 1982.

[6] Mathew, J., and Lai, F. C., "Enhanced Heat Transfer in a Horizontal Channel with Double Electrodes," *Conference Records of the 1995 IEEE Industry Applications Society 30th IAS Annual Meeting*, Vol. 2, Institute of Electrical and Electronics Engineers, Piscataway, NJ, 1995, pp. 1472–1479.

[7] Lai, F. C., "Effects of Buoyancy on EHD-Enhanced Forced Convection in a Horizontal Channel," *Journal of Thermophysics and Heat Transfer*, Vol. 12, No. 3, 1998, pp. 431–436.

[8] Huang, M., and Lai, F. C., "Numerical Study of EHD-Enhanced Forced Convection Using Two-Way Coupling," *Journal of Heat Transfer*, Vol. 125, No. 3, 2003, pp. 760–764.

[9] Tan, K. T., and Lai, F. C., "EHD-Enhanced Natural Convection in an Enclosure: Effects of Non-Symmetric Electric Field," *Proceedings of*

the 2001 National Heat Transfer Conference [CD-ROM], American Society of Mechanical Engineers, New York, 2001.

[10] Davidson, J. H., Kulacki, F. A., and Dunn, P. F., *Convective Heat Transfer with Electric and Magnetic Field, Handbook of Single-Phase Convective Heat Transfer*, edited by S. Kakaç, R. K. Shah, and W. Aung, Wiley, New York, 1987, Chap. 9.

[11] Huang, M., "EHD-Enhanced Heat and Mass Transfer," Ph.D. Dissertation, Univ. of Oklahoma, Norman, Oklahoma, 2005.

[12] Yamamoto, T., and Velkoff, H. R., "Electrohydrodynamics in an Electrostatic Precipitator," *Journal of Fluid Mechanics*, Vol. 108, July 1981, pp. 1–8.

[13] McDonald, J. R., Smith, W. B., Spencer H. W., and Sparks, L. E., "A Mathematical Model for Calculating Electrical Conditions in Wire-Duct Electrostatic Precipitation Devices," *Journal of Applied Physics*, Vol. 48, No. 6, 1977, pp. 2231–2243.

[14] Schinkel, W. M. M., Linhorst, S. J. M., and Hoogendoorn, C. J., "The Stratification in Natural Convection in Vertical Enclosures," *Journal of Heat Transfer*, Vol. 105, No. 2, 1983, pp. 267–272.

[15] Berkovsky, B. M., and Polevikov, V. K., "Numerical Study of Problems on High-Intensive Free Convection," *Heat Transfer and Turbulent Buoyant Convection*, edited by D. B. Spalding, and N. Afgan, Hemisphere, Washington, D.C., 1986, pp. 443–455.